Density of states in granular media in the presence of damping

David Linton Johnson,[1,*] Yanqing Hu,[2,†] and Hernan Makse[2]
[1]*Schlumberger Doll Research, One Hampshire Street, Cambridge, Massachusetts 02139, USA*
[2]*Levich Institute and Physics Department, City College of New York, New York, New York 10031, USA*
(Received 31 March 2015; published 11 June 2015)

We consider the density of states of granular media in which each grain-grain contact is damped with a damping force proportional to the relative velocity of the two grains, in addition to the usual spring constant. Under the assumption that the so-called criterion of proportional damping is only weakly violated we are able to deduce the density of states for undamped frequencies from the measured complex-valued frequencies of damped oscillations. We deduce a quantitative estimate of the deviation from the proportional criterion. We consider, specifically, numerical simulations of cases in which the grains are frictionless spheres that interact via Hertz central forces and all the nonzero contacts are damped with the same damping constant. We show how these ideas can be applied to data on real granular systems.

DOI: 10.1103/PhysRevE.91.062208 PACS number(s): 45.70.−n, 45.50.−j, 46.40.Ff

I. INTRODUCTION

In this article we consider the density of states of granular media in the presence of damping. We develop a theory that, subject to the validity of the assumed approximation, allows one to deduce what the density of states of an undamped system would be, from the measured complex-valued frequencies. The density of states of undamped granular media has received much attention in recent years, especially in its connection with the jamming transition [1–6]. Liu *et al.* [7] have written a review article on the topic. The idea is that a system jammed under the influence of a static stress induces a static deformation at the grain-grain contacts, each of which thus acquires a nonzero stiffness for subsequent small-amplitude deformations. One may thereby calculate the normal modes of vibration under the assumption that the system may be in the linear regime of small-amplitude vibrations. Such calculations assume the force versus displacement law for each contact follows from some specific law such as the Hertz/Hertz-Mindlin, or Hooke, or Lennard-Jones laws. Such calculations neglect the effects of damping at the grain-grain contacts. In experiments on real granular media, however, damping can be an important component of the dynamics [8]. Indeed, granular media can very effectively dampen the vibrations of metal structures having grain-filled cavities within themselves (see Ref. [9] and references therein). Moreover, Ref. [8] (and references therein) shows how it is possible to deduce accurate values of the complex-valued normal mode frequencies of a granular aggregate from measurements of the so-called effective mass of the granular medium.

The purpose of the present article is to show how it may be possible to deduce the density of undamped vibrational states of a granular system from the measured complex-valued normal mode frequencies that one has for damped systems. We base our results on our own previously published numerical simulations [10,11] of damped vibrations in granular media, under stress, in which the grains interact via Hertzian normal forces and via a damping mechanism proportional to the relative velocity of the grain centers. Although the intergranular force is a nonlinear function of contact displacement, we linearize around the equilibrium point to compute the normal mode frequencies relevant to small-amplitude vibrations.

There are situations in which there is no small-amplitude regime, whereby strictly linear equations of motion for the departure from equilibrium are valid. Schreck *et al.* [12] have pointed out that for granular systems interacting via strictly one-sided repulsive forces there is always a distribution of noncontact gaps extending continuously to zero, such that in the thermodynamic limit the smallest amplitude of vibration will open and close such a gap, which is intrinsically nonlinear. In the present article we assume that in damped granular media this situation does not arise. We assume that the forces of adhesion and adsorption that are the origin of the damping also ensure that each grain-grain contact has a linear operating regime, around the equilibrium configuration.

The article is organized as follows. We review a general theory of vibrational-libration normal modes of damped granular media in Sec. II. Because we intend our results ultimately to be applied to experimental results on real systems, the intergranular forces in this section include both normal and tangential components of the elastic and the damping forces. Here, we also present some previously published exact results relevant to the present work and we derive a new perturbation theory with which we can ultimately compute the undamped density of states. In Sec. III we describe how we performed our calculations of normal mode frequencies in a system of spherical grains interacting via damped Hertzian contact forces, i.e., normal forces only. The system is compressed under the action of the directional force of gravity. We present our new results on the density of states in Sec. IV. The conclusions are summarized in Sec. V.

II. THEORY

In this Section we review the assumed general equations of motion whose solutions determine the normal modes of the granular medium. We quote some relevant exact results and we also show the consequences of assuming the proportional approximation for the damping matrix. We end this section

*johnson10@slb.com
†Present address: School of Information Science and Technology, Sun Yat-sen University, Guangzhou 510006, China.

with our derivation of a perturbation theory that we employ to analyze our numerical simulations.

A. General considerations

Let $\mathbf{X}_i$ be the equilibrium position of the center of mass of the ith particle, whose mass is m_i, and $\mathbf{u}_i$ be its displacement from equilibrium. Similarly, $\boldsymbol{\theta}_i$ is the librational angle of rotation. If two neighboring particles translate or rotate such that their points of contact would move relative to each other there will be a restoring force due to the contact forces. The linearized equation of motion for the ith particle is

$$-m_i\omega^2\mathbf{u}_i = \sum_j \mathbf{K}_{ij}\cdot[\mathbf{u}_j + \boldsymbol{\theta}_j\times\mathbf{d}_{ji} - \mathbf{u}_i - \boldsymbol{\theta}_i\times\mathbf{d}_{ij}], \quad (1)$$

where $\mathbf{d}_{ij}$ is the vector from $\mathbf{X}_i$ to the point of contact with the jth grain. It is understood that the tensor $\mathbf{K}_{ij}(\equiv\mathbf{K}_{ji})$ is nonzero only for grains actually in contact with each other. (For simplicity we assume there is at most one contact per pair.)

The equation of motion for the angular variables is

$$-\omega^2\mathbf{I}_i\cdot\boldsymbol{\theta}_i = \sum_j \mathbf{d}_{ij}\times\mathbf{K}_{ij}\cdot[\mathbf{u}_j + \boldsymbol{\theta}_j\times\mathbf{d}_{ji} - \mathbf{u}_i - \boldsymbol{\theta}_i\times\mathbf{d}_{ij}], \quad (2)$$

where $\mathbf{I}_i$ is the moment of inertia tensor for the ith particle. These equations of motion, Eqs. (1) and (2), were originally employed in an early attempt to understand the interplay between rotational and translational degrees of freedom in the normal modes of granular media [13].

It is understood that, generally, each of the elements of the tensors $\mathbf{K}_{ij}$ is complex-valued and frequency dependent, reflecting the microscopic origin of the dissipation. In this article we may take

$$\mathbf{K}_{ij}(\omega)\to\mathbf{K}_{ij} - i\omega\xi\mathbf{B}_{ij}, \quad (3)$$

in which the second term describes an interparticle force proportional to the difference in velocity of the two grains. $\mathbf{K}$ and $\mathbf{B}$ are taken as real-valued and frequency independent. The parameter ξ monitors the strength of the damping. If we think of damping as being controlled by the viscosity of a fluid in the grain-grain contact, ξ is a stand-in for that viscosity. In this article we investigate how the normal mode frequencies evolve as ξ is varied. Note that this definition of $\mathbf{B}$ differs slightly from those in Refs. [10] and [11] in that here we explicitly factor out ξ from the definition.

Equations (1) and (2) have nontrivial solutions only for specific complex-valued frequencies ω_n. They may be combined as

$$\left[-\omega_n^2\mathbf{M} - i\omega_n\xi\mathbf{B} + \mathbf{K}\right]\mathbf{e}_n = 0, \quad (4)$$

where $\mathbf{e}_n$ is the combined vector of normal mode component displacements $\mathbf{u}_i$ and librations $\boldsymbol{\theta}_i$, $\mathbf{M}$ is the inertial tensor consisting of either the mass of a grain or the relevant component of the moment of inertia. $\mathbf{B}$ and $\mathbf{K}$ have been suitably generalized to this new notation.

Because the kinetic energy of the grains is always positive, the eigenvalues of $\mathbf{M}$ are also all positive. Therefore, the matrix $\mathbf{M}^{-1/2}$ can be defined and we can re-write Eq. (4) as

$$\left[-\omega_n^2\mathbf{I} - i\omega_n\xi\tilde{\mathbf{B}} + \tilde{\mathbf{K}}\right]\tilde{\mathbf{e}}_n = 0. \quad (5)$$

Here we have defined $\tilde{\mathbf{e}}_n \equiv \mathbf{M}^{1/2}\mathbf{e}_n$, $\tilde{\mathbf{B}} \equiv \mathbf{M}^{-1/2}\mathbf{B}\mathbf{M}^{-1/2}$, and $\tilde{\mathbf{K}} \equiv \mathbf{M}^{-1/2}\mathbf{K}\mathbf{M}^{-1/2}$.

Next, we investigate the trajectories of the normal mode frequencies, ω_n, as the damping parameter ξ is varied $\omega_n = \omega_n(\xi)$. Regardless of the value of $\xi > 0$, the imaginary part of any normal mode frequency is always negative, $\Im\{\omega_n(\xi)\} < 0$, corresponding to a mode that exponentially decays in time. Moreover, for every underdamped normal mode frequency in the fourth quadrant, ω_n^+, there is another in the third quadrant, $\omega_n^- = -(\omega_n^+)^*$, where * signifies complex conjugation, which is obvious from the structure of Eq. (4). There may also be overdamped normal modes for which $\omega_n^\pm$ are imaginary valued.

B. Exact results

If there is no damping, $\xi = 0$, then the real symmetric matrix $\tilde{\mathbf{K}}$ has positive eigenvalues ω_{n0}^2 and the undamped frequencies of oscillation for the corresponding normal modes $\mathbf{e}_{n0}$ are $\pm\omega_{n0}$. For small enough values of the damping one may do first-order perturbation theory with the result [8]

$$\omega_n^\pm = \pm\omega_{n0} - i\frac{\xi}{2}\frac{\tilde{\mathbf{e}}_{n0}^T\tilde{\mathbf{B}}\tilde{\mathbf{e}}_{n0}}{\tilde{\mathbf{e}}_{n0}^T\tilde{\mathbf{e}}_{n0}} + \mathcal{O}(\xi^2). \quad (6)$$

Each normal mode frequency initially moves perpendicular to the real axis from its starting point on the real axis.

For each trajectory, $\omega_n(\xi)$, there exists a critical value ξ_{nc}, which is finite, such that the mode becomes critically damped, i.e., ω_n is purely imaginary. For values of ξ approaching ξ_{nc} one has [10],

$$\lim_{\xi\to\xi_{nc}}\omega_n^\pm(\xi) = -i\lambda_n \pm g_n(\xi_{nc}-\xi)^{1/2} + \mathcal{O}(\xi-\xi_{nc})^1, \quad (7)$$

where λ_n and g_n are positive real numbers. Thus, the two branches $\omega_n^\pm(\xi)$ coalesce onto a single value on the negative imaginary axis at the critical damping. Their approach to $-i\lambda_n$ as $\xi\to\xi_{nc}^-$ is perpendicular to that axis. As ξ increases above the critical value the two roots remain imaginary and move apart from $-i\lambda_n$.

C. Proportional damping

In the very special case known as proportional damping [14] the matrix of damping parameters, $\mathbf{B}$, is everywhere proportional to the matrix of stiffness constants, $\mathbf{K}$. We may subsume this proportionality constant into the definition of ξ and write

$$\tilde{\mathbf{B}} = \tilde{\mathbf{K}}. \quad (8)$$

The distribution of normal stiffness values, $k_N(x_{ij})$, is directly related to the distribution of interparticle normal forces via the distribution of deformation values, x_{ij}. Such a force distribution is well known to display an exponential tail and to be relatively homogeneous [15]. Therefore, Eq. (8) amounts to neglecting the inhomogeneities in the force distribution as an approximation for the elastic and damping matrices. If each contact stiffness value was replaced by the average thereof, Eq. (8) would be exact.

If Eq. (8) holds true then the solution to Eq. (5) is simple. Because $\tilde{\mathbf{e}}_{no}$ is now an eigenmode of $\tilde{\mathbf{B}}$ it is also an eigenmode of the entire problem. The result is

$$\omega_n^{\pm}(\xi) = \frac{-i\xi\omega_{n0}^2}{2} \pm \omega_{n0}\sqrt{1-\left(\frac{\xi\omega_{n0}}{2}\right)^2}. \tag{9}$$

This well-known result obeys the exact results presented in the previous subsection. One has $\xi_{nc} = \frac{2}{\omega_{n0}}$.

The trajectories of the normal modes under the condition of proportional damping are perfect circles with center at the origin up to the point each becomes overdamped:

$$|\omega_n^{\pm}(\xi)| = \omega_{n0} \quad \forall \xi \leqslant \xi_{nc} = \frac{2}{\omega_{n0}}. \tag{10}$$

Moreover, the locus of all the (underdamped) normal mode frequencies for a given value of ξ is also a circle. The radius is $1/\xi$ and the center is at $-i/\xi$ [8,10]:

$$|\omega_n^{\pm}(\xi) + i/\xi| = 1/\xi \quad \forall n\ s.t.\ \xi \leqslant \xi_{nc} = \frac{2}{\omega_{n0}} \tag{11}$$

D. Perturbation theory

We now consider a situation, relevant to our numerical results, in which the proportional damping criterion, Eq. (8), is approximately true in the sense that departures from it are small:

$$\mathbf{B} = \mathbf{K} + \Delta\mathbf{B}. \tag{12}$$

We consider the effects of $\Delta\mathbf{B}$ to first order in perturbation theory. We make the substitutions $\mathbf{e}_{n0} \to \mathbf{e}_{n0} + \Delta\mathbf{e}_n$; $\omega_n(\xi) \to \omega_n(\xi) + \Delta\omega_n(\xi)$ in Eq. (4), or equivalently, Eq. (5), and collect all the terms that are first order in $\Delta\mathbf{B}$. We have

$$\begin{aligned} 0 = &\left(-\omega_n^2 - i\omega_n\xi\tilde{\mathbf{K}} + \tilde{\mathbf{K}}\right)\Delta\tilde{\mathbf{e}}_n \\ &+\Delta\omega_n(-2\omega_n - i\xi\tilde{\mathbf{K}})\tilde{\mathbf{e}}_{n0} - i\omega_n\xi\,\Delta\tilde{\mathbf{B}}\tilde{\mathbf{e}}_{n0}. \end{aligned} \tag{13}$$

Because the matrix $\mathbf{K}$ is real-symmetric, so is $\tilde{\mathbf{K}}$, which means that $\tilde{\mathbf{e}}_{n0}^T$ is a left eigenvector of $\tilde{\mathbf{K}}$, having the same eigenvalue, ω_{n0}^2. If we multiply Eq. (13) on the left by $\tilde{\mathbf{e}}_{n0}^T$ the first term on the right-hand side vanishes identically and we have our desired result:

$$\Delta\omega_n^{\pm}(\xi) = -\frac{i\omega_n^{\pm}(\xi)\xi\,\Delta\tilde{\mathbf{B}}_{n,n}}{2\omega_n^{\pm}(\xi) + i\xi\omega_{n0}^2} + \mathcal{O}(\Delta\tilde{\mathbf{B}})^2, \tag{14}$$

where

$$\Delta\tilde{\mathbf{B}}_{n,n} = \frac{\tilde{\mathbf{e}}_{n0}^T\Delta\tilde{\mathbf{B}}\tilde{\mathbf{e}}_{n0}}{\tilde{\mathbf{e}}_{n0}^T\tilde{\mathbf{e}}_{n0}}. \tag{15}$$

With the use of Eq. (9) we may rewrite this in the form

$$\Delta\omega_n^{\pm}(\xi) = i\omega_n^{\pm}(\xi)\Delta\theta_n^{\pm}, \tag{16}$$

where

$$\Delta\theta_n^{\pm} = \mp\frac{\xi\,\Delta\tilde{\mathbf{B}}_{n,n}}{2\omega_{n0}\sqrt{1-\left(\frac{\xi\omega_{n0}}{2}\right)^2}}. \tag{17}$$

Equations (16) and (17) show that to first order in $\Delta\mathbf{B}$ an under-damped normal mode frequency moves by an angular amount $\Delta\theta_n^{\pm}$ along the same circular trajectory defined by Eq. (10):

$$|\omega_n^{\pm}(\xi) + \Delta\omega_n^{\pm}(\xi)| = \omega_{n0} + \mathcal{O}(\Delta\mathbf{B})^2. \tag{18}$$

We shall use Eq. (18) to deduce information about the distribution of undamped frequencies ω_{n0} from our data in the presence of damping under the assumption that deviations from the proportional damping criterion are weak.

We note in passing that for any of the overdamped modes Eq. (16) still holds, but both $\omega_n^{\pm}$ and $\Delta\theta_n^{\pm}$ are imaginary with the result that $\Delta\omega_n^{\pm}$ is also imaginary, which makes intuitive sense.

III. NUMERICAL SIMULATIONS

In previous publications [10,11] we reported the results of normal mode calculations of ensembles of granular media confined to a container. It is these results on damped granular media that we will use to deduce the density of states of the undamped system and so we recap them here. Our interests then were to gain some understanding of the properties of the so-called effective mass of granular media [8,16]. Accordingly, the particles in the simulations were not subjected to an isotropic confining pressure but, rather, they were subjected to a directional gravitational field, as per the experiments. The particles were identical spheres of mass m. We assumed the particles were frictionless and that they interact with their neighbors via the Hertz force [17]:

$$F_N = \tfrac{2}{3}k_n R^{1/2}x_{ij}^{3/2}, \tag{19}$$

where R is the radius and $x_{ij} > 0$ is the degree of compression of the center-to-center distance between sphere i and sphere j. (There is no force between noncontacting spheres.) After the spheres have settled into their equilibrium configuration, each contact has a different value of the static compression x_{ij}; those near the top of the container are compressed less than those near the bottom. Each contact responds to an infinitesimal additional distortion by means of a spring constant, which is given by

$$k^N(x_{ij}) = \frac{dF_N}{dx_{ij}} = k_n R^{1/2}x_{ij}^{1/2}. \tag{20}$$

In tensor notation, then, the expression for the 3×3 stiffness matrix between two contacting spheres is

$$\mathbf{K}_{ij} = k^N(x_{ij})\hat{\mathbf{d}}_{ij}\hat{\mathbf{d}}_{ij}, \tag{21}$$

where $\hat{\mathbf{d}}_{ij}$ is a unit vector pointing from one sphere center to the other and we are using dyadic notation.

We assumed the damping matrix $\mathbf{B}$ is of the same general form as Eq. (21) except that we assumed all the damping constants were the same for any two spheres in contact:

$$\mathbf{B}_{ij} = \langle k^N\rangle\hat{\mathbf{d}}_{ij}\hat{\mathbf{d}}_{ij}, \tag{22}$$

where $\langle k^N\rangle$ is the average of all the nonzero $k^N(x_{ij})$ values. The motivation behind this assumption was that we were attempting to understand the damping effects of adsorbed fluids at the grain-grain contacts, which are presumably insensitive to the degree of compression of the two grains.

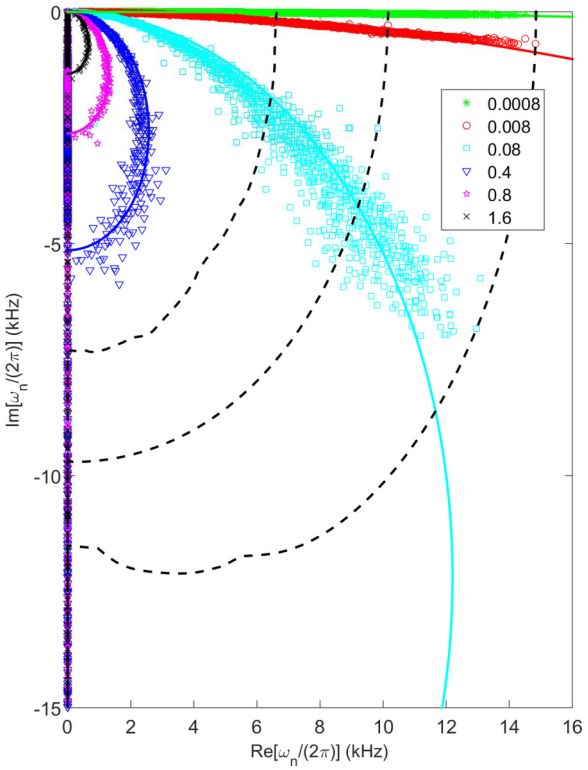

FIG. 1. (Color online) The complex-valued normal mode frequencies of the model granular medium for different values of the damping parameter, ξ. The legend gives the values of $2\pi\xi$ in milliseconds. The solid curves are circles of radius $1/(2\pi\xi)$ as per Eq. (11). The dashed lines are the trajectories of three of the normal mode frequencies as ξ is increased from zero to ξ_{nc} and beyond. All the modes are underdamped for the smallest three values of ξ, whereas for the others some of the modes are overdamped.

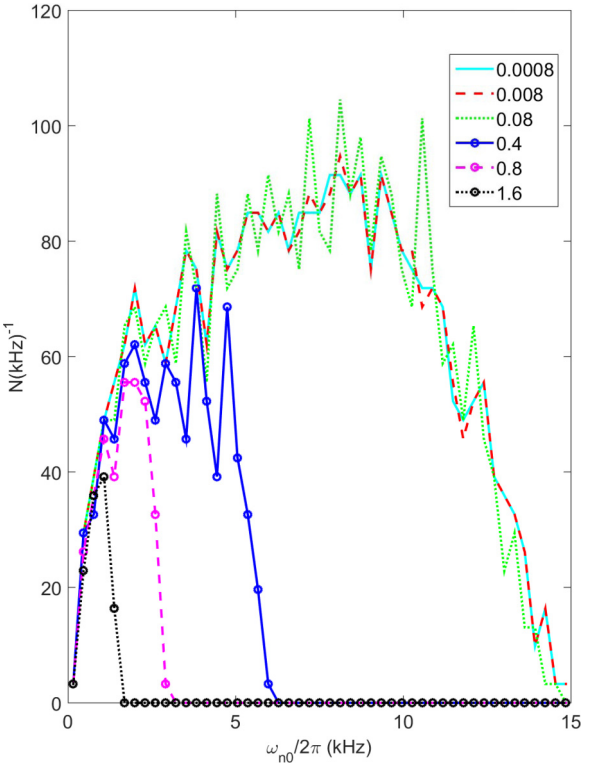

FIG. 2. (Color online) Density of undamped frequencies deduced from the underdamped frequencies of Fig. 1. All the modes for the smallest three values of ξ give results that essentially agree with each other. The partial densities of states for the remaining three overlap these results for low frequencies where $\omega_{n0} < 2/\xi$.

The complex-valued resonance frequencies of Eq. (4) are now computed from the eigenvalues $\{\lambda_n\}$ of the matrix $\mathbf{A}$, which is given in block form as

$$\mathbf{A} = \begin{pmatrix} \mathbf{0} & \mathbf{I} \\ -\mathbf{M}^{-1}\mathbf{K} & -\xi\mathbf{M}^{-1}\mathbf{B} \end{pmatrix}. \tag{23}$$

We have $\omega_n = i\lambda_n$. More details of the simulations may be found in Refs. [10] or [11]. In the limit of no damping, $\xi\mathbf{B} \to 0$, it is easy to prove that the eigenvalues are $\lambda_n = \pm i\omega_{n0}$. In the absence of damping, then, we retrieve exactly the same result as diagonalizing the dynamic matrix $\tilde{\mathbf{K}}$, as one would intuitively expect.

The results of our simulations, for different assumed values of ξ, are shown in Fig. 1 for a situation in which we simulated 314 spheres, giving rise to 1884 normal mode frequencies, the underdamped of which occur as pairs in the third and fourth quadrant. This figure is a more complete version of similar plots shown in Refs. [10] and [11]. Of these 1884 normal mode frequencies, 22 of them are essentially zero-frequency modes ($|\omega_{n0}| < 3 \times 10^{-7}$ kHz), which we do not include in the analysis. It is clear that $\mathbf{B} \neq \mathbf{K}$. Nonetheless, the consequences of Eq. (8) are reasonably well attained. Each trajectory is roughly a circle as per Eq. (10) and each obeys the exact results, Eqs. (6) and (7). The loci of all the frequencies is also approximately a circle, Eq. (11). All of the modes are underdamped for the three smallest values of ξ. Some of the modes are overdamped (ω_n is purely imaginary) for the other three values of ξ. (See the Supplemental Material [18] for a movie that shows the evolution of all the complex frequencies as ξ is continuously increased starting from zero.) The data lend themselves to an analysis with the perturbation theory described in Sec. II D.

IV. DENSITY OF STATES

Assuming the approximate validity of Eq. (18) it is easy to compute the density of undamped states, $N(\omega_{n0})$, from the measured underdamped frequencies. The number of states that would have an undamped frequency between ω_{n0} and $\omega_{n0} + \Delta\omega_{n0}$ is equal to the number of actual modes for which $|\omega_n|$ lies within these limits, for the underdamped modes. Corrections to this are of order $\mathcal{O}(\Delta\mathbf{B})^2$. We have binned all the underdamped frequencies shown in Fig. 1 accordingly. The results are shown in Fig. 2. For the three smallest values of ξ all of the normal modes are underdamped and the resultant density of states for each of these data sets agrees with the others. The partial density of states computed from the simulations corresponding to the three largest values of ξ are also in agreement with the other three. This agreement is due, evidently, to the perturbation theory result, Eq. (18).

We note that our results for the undamped density of states do not exhibit the well-known low-frequency plateau

characteristic of the density of states in jammed systems reported by others [1–7]. We attribute this to the several differences between our calculations and theirs. Our system is not intended to model a macroscopically infinite system. Rather, we are modeling the normal modes of a rigid cup, loosely filled with grains. There is a rigid bottom plane and the top has a finite extent. Two of the side walls are also rigid; the remaining direction has periodic boundary conditions. Perhaps the most obvious difference is that we have included a constant downward force on each sphere, intended to mimic the force of gravity. Thus, the spheres toward the bottom are compressed more than those near the top and the system is macroscopically heterogeneous. So to say, the distance from the so-called J point varies continuously from top to bottom.

At this point we may push our luck and compute the contribution to the densities of undamped states from all the overdamped states, i.e., those on the negative imaginary axis. From Eq. (9) we have

$$\xi > \xi_{nc}\colon\ |\omega_n^{\pm}(\xi)| = \frac{\xi\omega_{n0}^2}{2} \mp \omega_{n0}\sqrt{\left(\frac{\xi\omega_{n0}}{2}\right)^2 - 1} + \mathcal{O}(\Delta\mathbf{B})^1, \tag{24}$$

which can be inverted:

$$\omega_{n0} = \frac{|\omega_n^{\pm}(\xi)|}{\sqrt{\xi|\omega_n^{\pm}(\xi)| - 1}} + \mathcal{O}(\Delta\mathbf{B})^1. \tag{25}$$

The overdamped modal frequencies order as $|\omega_n^+(\xi)| < 2/\xi < |\omega_n^-(\xi)|$. We convert each value of $|\omega_n^-(\xi)|$ into its undamped value according to Eq. (25) and compute the contributions of these frequencies to a partial density of states. The results for the three data sets that have overdamped modes are shown in Fig. 3. They agree with each other for frequencies $\omega_{n0} > 2/\xi$. This is quite surprising because Eq. (24) has errors of order $(\Delta\mathbf{B})^1$, unlike Eq. (18).

Pushing our luck further again we plot the total density of states $N_{\text{total}} = N + N_{\text{overdamped}}$ in Fig. 4. Remarkably, all six data sets, corresponding to damping parameters ξ, which range over a factor of 2000, stack on top of each other. We conclude that we have identified a way to deduce the density of undamped states from measurements of those states that are possibly heavily damped.

Finally, we use Eq. (17) to deduce some information about the degree to which the proportional damping condition, Eq. (8), is violated. The situation is demonstrated graphically in Fig. 5 where we have highlighted one datum for analysis; the data set corresponds to $2\pi\xi = 0.4$ from Fig. 1. Were the proportional damping criterion to hold exactly, this point would lie on the intersection of the two circles given by Eq. (10) (the dashed curve) and Eq. (11) (the solid curve). (For some of the underdamped frequencies the two curves do not intersect and are excluded from the analysis.) The angular deviation, $\Delta\theta_n$, between this point and the actual location is related to the deviation from the proportional criterion by Eq. (18), to first order. It is simple enough to solve for $\Delta\tilde{\mathbf{B}}_{nn}$ for each data point. The results are plotted in Fig. 6 as a function of the presumed value of ω_{n0} for each trajectory, for each of the six data sets.

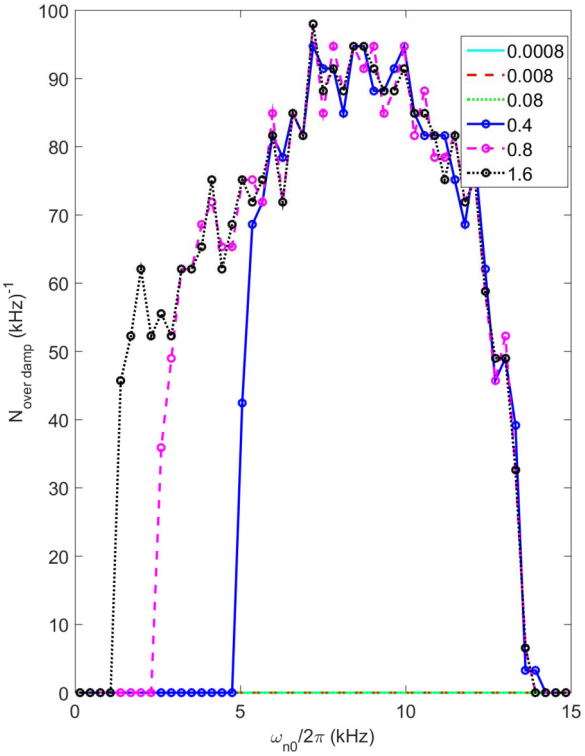

FIG. 3. (Color online) Density of undamped frequencies deduced from the overdamped frequencies of Fig. 1. Only three of the data sets, corresponding to the largest values of ξ, have overdamped modes.

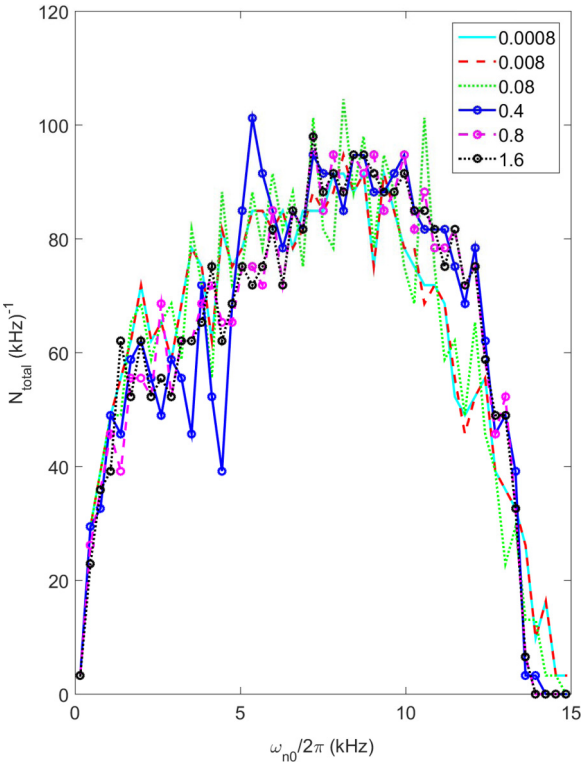

FIG. 4. (Color online) Total density of states of the modes whose complex-valued frequencies are shown in Fig. 1. Each curve is the sum of the relevant curves in Figs. 2 and 3. These six curves are essentially all the same.

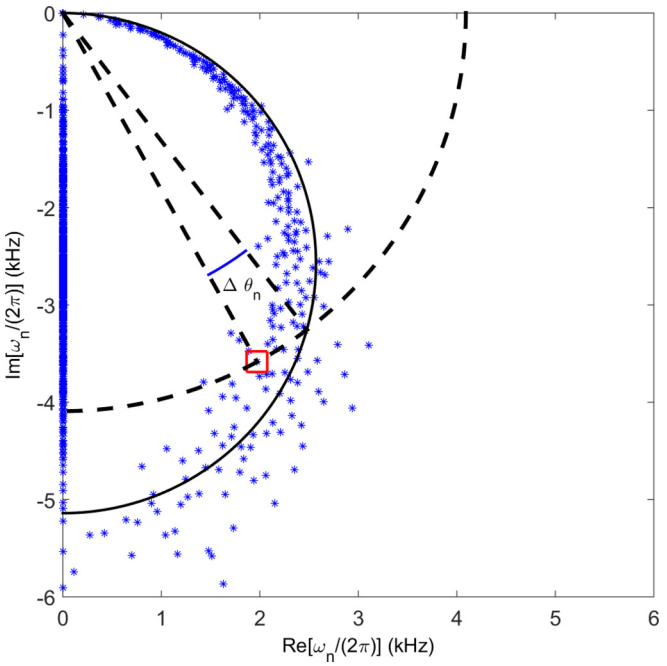

FIG. 5. (Color online) Graphical illustration of $\Delta\theta_n$. The data set corresponds to $2\pi\xi = 0.4$ from Fig. 1 and one of those data points is isolated. The dashed curve is a circle of radius $|\omega_n|$ passing through that point. The solid curve is a circle of radius $(2\pi\xi)^{-1}$ as per Eq. (11). The difference between the actual location of the normal mode frequency and the intersection of these two circles defines $\Delta\theta_n$, as indicated. In this example, $\Delta\theta_n < 0$.

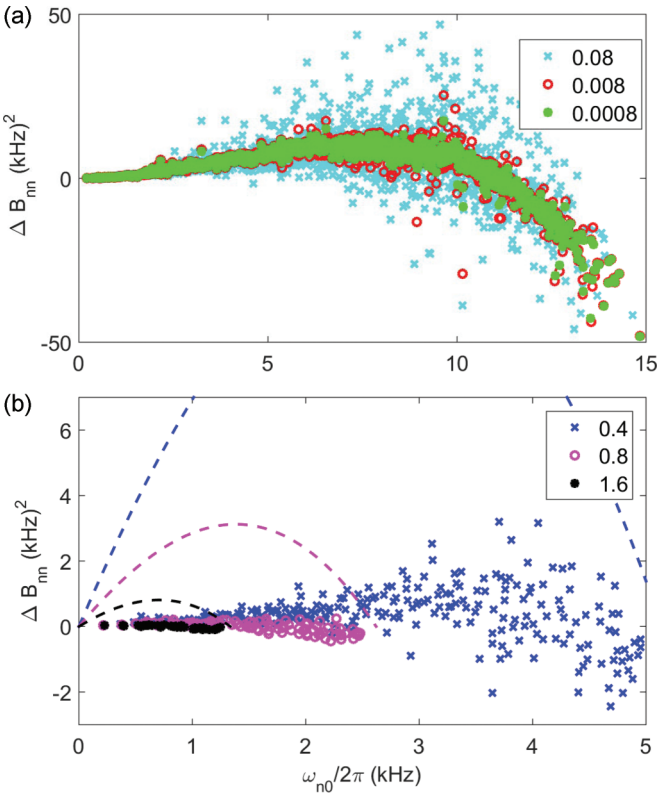

FIG. 6. (Color) Deduced values of $\Delta\tilde{\mathbf{B}}_{nn}$ cross-plotted against $|\omega_n| \approx \omega_{n0}$. (a) The lowest three values of damping, ξ, for which all the modes are underdamped. (b) The remaining three values of ξ for which some of the modes are overdamped. For these data sets we can deduce $\Delta\tilde{\mathbf{B}}_{nn}$ only for the underdamped of those modes. Note the change of scale in the axes for the two plots. The dashed curves demonstrate the maximum value of $\tilde{\mathbf{B}}_{nn}$ that can be deduced with our technique.

We have plotted the results for the three least damped systems in the top panel; the other three are plotted in the bottom panel. There are several interesting features to these results. First, we see that the results for $2\pi\xi = 0.0008$ and $2\pi\xi = 0.008$ virtually overlie each other. That for $2\pi\xi = 0.08$ is consistent with these two but has a larger spread in apparent $\Delta\tilde{\mathbf{B}}_{nn}$ values. This may indicate the breakdown of the first-order perturbation theory, though we have already seen that the density of states calculation is still robust. The spread is noticeably smaller for ω_{n0} less than 5 kHz in all three data sets. There is a noticeable systematic variation of $\Delta\tilde{\mathbf{B}}_{nn}$ with ω_{n0} in all three sets.

The situation is significantly different for the case of the three largest values of the damping parameter, ξ, which are shown in the lower panel of Fig. 6. Obviously, only those underdamped modes for which the two circles, Eqs. (10) and (11), have an intersection are those that can be analyzed. Even so it is surprising to us that the surviving values of $\Delta\tilde{\mathbf{B}}_{nn}$ are so much smaller than those in the top panel of the figure. In almost all cases we have $\tilde{\mathbf{B}}_{nn} \ll \tilde{\mathbf{K}}_{nn} = \omega_{n0}^2$ as would be a necessary condition for the validity of first-order perturbation theory.

We note, however, from Eq. (9), that there is a simple relation between the polar angle, θ_n, and the damping parameter, ξ, when the proportional damping criterion holds:

$$\sin(\theta_n^{\pm}) = -\frac{\xi\omega_{n0}}{2}. \tag{26}$$

This, in turn, implies $\theta_n^{\pm}(\xi) \to -\pi/2$ with infinite slope as $\xi \to \xi_{nc} = 2/\omega_{n0}$. But Eq. (17) indicates that corrections to Eq. (26) due to the breakdown of the proportional damping approximation themselves diverge in this limit. Thus, a more appropriate condition for the validity of first-order perturbation theory might be the more restrictive relation $|\frac{d\Delta\theta_n^{\pm}}{d\xi}| \ll |\frac{d\theta_n^{\pm}}{d\xi}|$. This restriction would imply that the validity of Eq. (17) should be restricted to $\xi \ll \xi_{nc}$. We see from Eq. (17) that solving for $\tilde{\mathbf{B}}_{nn}$ from the measured $\Delta\theta_n$ values will tend to collapse $\tilde{\mathbf{B}}_{nn}$ to small values, for heavily damped systems.

It is clear from Fig. 5 and Eq. (17) that if $\Delta\tilde{\mathbf{B}}_{nn}$ is large enough the computed $\Delta\theta_n$ would mean the resonance frequency would lie on the negative imaginary axis. For larger values of $\Delta\tilde{\mathbf{B}}_{nn}$ the modes would be overdamped and Eq. (17) would be meaningless. These boundaries are indicated with the dashed lines in Fig. 6.

These ideas can, at least in principle, be applied to real experimental data on granular systems. If the number of measurable frequencies is large enough a cross-plot of those frequencies in the complex plane could allow one to deduce the approximate value of ξ, assuming the proportional damping model has approximate validity. This was partially accomplished in Fig. 7 of Ref. [10] in which previously

published experimental data were shown to cluster around the circle defined by Eq. (11), although the existing data covered only a small fraction of that circle. The contribution to the undamped density of states from the underdamped modes does not require a knowledge of ξ but the contribution from the overdamped modes does require it as does any estimate of the deviation, $\Delta\tilde{\mathbf{B}}_{nn}$, from the proportional damping criterion.

V. CONCLUSIONS

We have presented a way of analyzing normal mode frequencies of granular media in situations where these frequencies are complex-valued due to damping. We have argued that in cases in which the so-called proportional damping criterion is weakly violated one may reconstruct the density of undamped states from the measured complex-valued frequencies. Furthermore, we have shown how one may deduce specific information about the relevant matrix elements of the damping matrix that relate to deviations from strictly proportional behavior. The ideas presented here work reasonably well on numerical simulations of the normal modes of a collection of spheres interacting via Hertz contacts for the stiffness and with the assumption that all the contacts are damped the same. We have shown how these ideas can be applied to data on real granular systems, assuming one is able to measure a significant number of those frequencies.

ACKNOWLEDGMENT

We thank the NSF (Grant No. DMR-1308235) and DOE Geosciences Division (Grant No. DE-FG02-03ER15458) for financial support.

[1] C. S. O'Hern, L. E. Silbert, A. J. Liu, and S. R. Nagel, Phys. Rev. E **68**, 011306 (2003).
[2] L. E. Silbert, A. J. Liu, and S. R. Nagel, Phys. Rev. E **79**, 021308 (2009).
[3] C. Zhao, K. Tian, and N. Xu, Phys. Rev. Lett. **106**, 125503 (2011).
[4] M. Wyart, L. E. Silbert, S. R. Nagel, and T. A. Witten, Phys. Rev. E **72**, 051306 (2005).
[5] M. Wyart, S. R. Nagel, and T. A. Witten, Europhys. Lett. **72**, 486 (2005).
[6] N. Xu, M. Wyart, A. J. Liu, and S. R. Nagel, Phys. Rev. Lett. **98**, 175502 (2007).
[7] A. J. Liu, S. R. Nagel, W. van Saarloos, and M. Wyart, in *Dynamical Heterogeneities in Glasses, Colloids, and Granular Media*, edited by L. Berthier, G. Biroli, J.-P. Bouchaud, L. Cipelletti, and W. van Saarloos (Oxford University Press, Oxford, 2011).
[8] J. Valenza and D. L. Johnson, Phys. Rev. E **85**, 041302 (2012).
[9] J. Valenza, C.-S. Hsu, and D. L. Johnson, J. Acoust. Soc. Am. **128**, 2768 (2010).
[10] Y. Hu, D. L. Johnson, J. J. Valenza, F. Santibanez, and H. A. Makse, Phys. Rev. E **89**, 062202 (2014).
[11] Y. Hu, D. L. Johnson, J. J. Valenza, and H. Makse, Geophysics **79**, L41 (2014).
[12] C. F. Schreck, T. Bertrand, C. S. O'Hern, and M. D. Shattuck, Phys. Rev. Lett. **107**, 078301 (2011).
[13] L. M. Schwartz, D. L. Johnson, and S. Feng, Phys. Rev. Lett. **52**, 831 (1984).
[14] L. Meirovitch, *Fundamentals of Vibration* (Waveland Press, Long Grove, IL, 2001).
[15] H. A. Makse, D. L. Johnson, and L. M. Schwartz, Phys. Rev. Lett. **84**, 4160 (2000).
[16] C. J. Hsu, D. L. Johnson, R. A. Ingale, J. J. Valenza, N. Gland, and H. A. Makse, Phys. Rev. Lett. **102**, 058001 (2009); J. Valenza, C. J. Hsu, R. Ingale, N. Gland, H. A. Makse, and D. L. Johnson, Phys. Rev. E **80**, 051304 (2009).
[17] L. D. Landau and E. M. Lifschitz, *Theory of Elasticity* (Oxford University Press, Oxford, 1965).
[18] See Supplemental Material at http://link.aps.org/supplemental/10.1103/PhysRevE.91.062208 for a movie that shows how the normal mode frequencies evolve as ξ is continuously increased, starting from zero. For any value of ξ the red symbols indicate the corresponding current value of each eigenfrequency, and the blue symbols indicate all the frequencies for the previous values of ξ. Thus, one may see the evolution of all the trajectories of all the modes in the complex plane.